CO32–Mobility in Carbonate Apatite As Revealed by Density Functional Modeling

UNIVERSITÀ DEGLI STUDI DI TORINO

CO_3^{2-} Mobility in Carbonate Apatite as Revealed by Density Functional Modelling

*F. Peccati[1], M. Corno[1], M. Delle Piane[1], G. Ulian[2] , P. Ugliengo[1] and G. Valdrè[2]**

[1]Università di Torino, Dipartimento di Chimica and NIS (Nanostructured Interfaces and Surfaces Centre), Via Pietro Giuria 7, 10125 Torino – Italy

[2]Università di Bologna "Alma Mater Studiorum", Dipartimento di Scienze Biologiche, Geologiche e Ambientali, Centro di Ricerche Interdisciplinari di Biomineralogia, Cristallografia e Biomateriali, Piazza di Porta San Donato 1, 40126 Bologna – Italy

Corresponding author: giovanni.valdre@unibo.it; Tel:+390512094943

Abstract

Carbonate apatite is a material of the utmost importance as it represents the inorganic fraction of biological hard tissues in bones and teeth. Here we study the static and dynamic features of CO_3^{2-} ion in the apatitic channel of carbonate apatite (A-type substitution), by applying both static and dynamic quantum mechanical calculations based on density functional methods with B3LYP-D* and PBE functionals. The static calculations reveal a number of almost energetically equivalent carbonate configurations in the channel, leading to cell parameters compatible with the $P\bar{3}$ space group assigned by the experimental X-ray structure determination. *Ab initio* isothermal-isobaric molecular dynamics simulations provide insights on the CO_3^{2-} mobility, showing that, at the temperature of the experimental structural determination, the CO_3^{2-} moiety undergoes a dynamic disorder, as the carbonate group is almost free to move within the apatitic channel enhancing its exchangeability with other anions.

Keywords: Biological tissue, biomaterials, carbonate substitution, PBE, B3LYP-D*, AIMD.

Introduction

Apatites have drawn substantial attention from the biological point of view because they represent the primary inorganic constituents of biological hard tissue, particularly in the form of carbonate-containing hydroxyapatite ($Ca_{10}(PO_4)_{6-2y}(OH)_{2-2x}(CO_3)_{x+3y}$) nanocrystals.[1] Spectroscopic data indicate that bone apatite contains just a small or even negligible concentration of hydroxyl groups, whereas the presence of carbonate groups is clearly remarked.[2] The composition of bioinorganic materials is of the utmost importance in determining their properties and therefore the carbonate substitution is fundamental for the features of bone tissue. In particular, the carbonate content of bone and teeth tissues is compatible with the stoichiometry of the so-called A-type carbonate apatite (chemical formula $Ca_{10}(PO_4)_6CO_3$, structure in Figure 1), in which the carbonate group is accommodated in a channel of calcium ions (the apatitic channel), giving a CO_3^{2-} for OH^- substitution.[2] This structure is particularly interesting due to the multiple configurations for the CO_3^{2-} reported by XRD analyses.[3-5] Indeed, experimental data assign this structure to the $P\bar{3}$ space group,[5] incompatible with previous theoretical results stating that the system has no symmetry (*P1* space group).[6] In particular, calculated and experimental data are in disagreement upon cell parameters.[6-8] Moreover, classical molecular dynamics simulations indicate that the carbonate has a certain rotational freedom in the lattice,[9] which should allow a remarkable mobility of this group at room temperature. The aim of this work is to understand and to overcome the difference between calculated and experimental results using accurate static and dynamic *ab initio* computational tools.

Computational Details

All the calculations were done within the Density Functional Approximation (DFT). The Perdew, Burke and Enzerhof GGA (Generalized Gradient Approximation) exchange-correlation functional (PBE) was adopted for the molecular dynamics simulations,[10] while for static calculations the hybrid Becke, three parameters, Lee-Yang-Parr (B3LYP) functional was chosen.[11,12]

A developmental version of the CRYSTAL09 code[13-15] was adopted for the static calculations in its massively parallel version.[16,17] The chosen Gaussian basis set was the same already employed by some of us in recent *ab initio* simulations of apatites:[6,18] an all-

electron 8-6511G(2d) basis set for Calcium, a 85-21G(d) basis set for Phosphorous, a 6-31G* basis set for Oxygen and a 6-21G* basis set for Carbon. Values of the tolerances that control the truncation criteria for the bielectronic Kohn-Sham integrals were set to ITOL1 = ITOL2 = ITOL3 = ITOL4 = 7, while the remaining value of tolerance, ITOL5, was changed to 16. The Hamiltonian matrix was diagonalized at 36 *k* points in the first Brillouin zone.[19] Internal coordinates were optimised using the analytical gradient method and the Hessian matrix was upgraded with the Broyden-Fletcher-Goldfarb-Shanno (BFGS) algorithm. Tolerances for the maximum allowed gradient and the maximum atomic displacement for considering the geometry as converged were kept at the default values (0.00045 Hartree $Bohr^{-1}$ and 0.00030 Bohr, respectively).

Harmonic frequencies were calculated with CRYSTAL and the infrared intensity for each normal mode was obtained by computing the dipole moment variation along the normal mode, adopting the Berry phase method.[20] When not otherwise specified, harmonic frequencies were computed for the carbonate group only, considered as an independent fragment within the structure.

A general drawback of all common GGA functionals, including hybrids, is that they cannot describe van der Waals (dispersive) forces. Since dispersion plays a key role in many chemical systems, it was necessary to apply a correction to the energy obtained with the standard density functional methods. For the B3LYP static calculations presented in this work, the modification proposed by Civalleri *et al.* to the Grimme's standard set of parameters[21] was adopted and referred in the following with the D* labeling.[22] This correction, when activated during a geometry optimization, is added to the energy and its gradient to determine the final geometry. Carbonate apatite is a highly ionic structure, particularly for the Ca ion which is expected to be very little polarizable. To account for that, the Grimme's original Ca dispersion C_6 parameter was set to zero, thus entirely neglecting its contribution to dispersive interactions. This approximation led to a better agreement with structural experimental data (data not reported).

Ab initio molecular dynamics (AIMD) simulations were performed using the CP2K code.[23] The Quickstep technique[24] with a mixed plane wave and Gaussian basis set methodology (Gaussian and Plane Wave method, GPW)[25] was employed to calculate the electronic structure. We used the PBE functional, with the Goedecker-Teter-Hutter pseudopotentials[26] and a double-ζ basis set with polarization functions (DZVP). The cutoff

for the plane wave basis was set to 400 Ry. AIMD simulations were run at 300 K in the isothermal–isobaric ensemble (NPT), at 0 external pressure using a flexible cell. A time step of 0.5 fs was chosen. A reference cell was set, to avoid unphysical jumps in energy. The canonical sampling through velocity rescaling (CSVR) thermostat was employed, with a 10 fs time constant.[27]

Results

Static calculations: geometrical and vibrational features

A previously published model of fully carbonate A-type CAp ($Ca_{10}(PO_4)_6CO_3$) was used as reference geometry (Figure 1) for the calculations presented in this work.[6] This structure, in turn, was obtained by modeling the substitution of two hydroxyl ions by a carbonate ion in the unit cell of hydroxyapatite ($Ca_{10}(PO_4)_6(OH)_2$).[28] In A-type CAp the carbonate ion is located in the apatitic channel, in an intermediate position between the two substituted hydroxyl ions, and is in the so-called A1 ("closed") configuration, with two oxygen atoms close to the *c* axis.

From the quantum chemical point of view, it is not possible to impose to this structure the $P_{\bar{3}}$ space group proposed by Fleet and Liu[29], because symmetry operators would generate six non-physical rotational replicas of the carbonate group around the *c* axis within the same unit cell. The $P_{\bar{3}}$ group should therefore imply that the experimental structure results either from a static disorder of the carbonate group differently oriented in diverse crystal domains or from a dynamic disorder in which the available minimum positions are frequently visited due to easily surmountable barriers for carbonate rotation around the *c* axis. Such minimum configurations have been searched by a rotational scan of 360° degrees around the axis of the carbonate ion parallel to the *c* axis, with a step of ~6°, starting from the reference geometry, followed by a full optimization of the resultant models. Optimization led to twelve minimum energy structures covering the whole circumference, as shown in Figure 2. In each of the twelve structures, the carbonate group is surrounded by the six calcium ions of the apatitic channel. These ions are arranged in a fairly regular octahedral coordination, with the octahedron only slightly elongated along the direction taken up by the carbonate oxygen perpendicular to the *c* axis. This distortion from regularity, consequent to the introduction of the carbonate ion in the apatitic unit cell, is

responsible for the symmetry breaking with respect to hydroxyapatite. It results also in a significant rotation of the adjacent phosphate groups dependently on the carbonate orientation (Figure 2): repulsive interactions between carbonate and phosphate oxygen atoms play an important role in determining the allowed configurations of the carbonate ion.

Relative energies and cell parameters of the structures are reported in Table 1. As can be immediately seen, energy differences among the structures are very low, the highest being 2.85 kJ/mol. In particular, structures labeled with odd numbers are the lowest in energy (differing by just 0.62 kJ/mol) and correspond to six different CO_3^{2-} configurations regularly spread over the circumference. These structures, which will be the most populated, account for the experimentally observed $P_{\bar{3}}$ space group of A-type CAp, reproducing the average distribution of the carbonate group over these configurations. Nevertheless, the six remaining structures (labeled with even numbers) are not so energetically different, and begin to be populated at room temperature. The lower energy structures correspond to a carbonate ion configuration where the carbonate oxygen atom perpendicular to the *c* axis is in an intermediate position between the two adjacent phosphate oxygen atoms, whereas higher energy structures correspond to a configuration where the carbonate oxygen is aligned with a single phosphate oxygen atom.

It is clear from the present results that the energy differences between CAp structures with different CO_3^{2-} orientations are somehow at the lowest limit of the accuracy that DFT calculations can provide. Nevertheless, the important message is that whatever the "right" energy difference between CAp structures characterized by different CO_3^{2-} orientations is, the present results indicate that the forces keeping the CO_3^{2-} moiety in place are very weak as also shown by dynamical calculations (vide infra). While dependency of the results on improving the basis set quality and the adopted functional is expected, this is not going to change the suggested physical picture on the high CO_3^{2-} mobility.

Despite the very small energy difference between the considered configurations, the orientation assumed by the carbonate group remarkably affects the *a* and *b* parameters of the unit cell, as reported in Figure 3, showing the trend of cell parameters and volume for the various models. The squares and circles in the topmost part of the graph refer to the cell parameters *a* and *b* respectively, and indicate the existence of an inverse relationship between these two quantities, since the first one increases as the second decreases, and *vice*

versa. The parameter *c* (triangles) and the cell volume (stars), on the other hand, remain fairly constant throughout all the structures. These data indicate that the unit cell of A-type carbonate apatite responds in a rather subtle way to the orientation of the carbonate ion. Thus, it is patent that the experimentally observed structure (where the parameters *a* and *b* are equal) is an average of all the possible carbonate ion configurations. Since the positioning of the carbonate ion among the various configurations is expected to follow the Boltzmann distribution, the generic average cell parameter $<x>$ may be obtained by the equation:

$$< x >= \frac{\sum_{i=1}^{n} x_i \exp\left(-\frac{\Delta E_i}{k_B T}\right)}{\sum_{i=1}^{n} \exp\left(-\frac{\Delta E_i}{k_B T}\right)}$$

where n is the number of considered structures (n=12) and ΔE_i is the difference in energy between structure i and the most stable one. Averaging over the twelve configurations leads to values in better agreement with experimental data than those of the single structures, so that *a* and *b* parameters almost coincide. Moreover, average cell angles result in a good agreement with the angles required by the space group $P_{\bar{3}}$ (Table 1). This confirms that the observed A-type carbonate apatite structure is indeed an average of multiple structures resulting from the disordering of the carbonate ion around the *c* axis.

The role of dispersive interactions was assessed by re-optimizing the CAp structures without including the Grimme correction: energy gaps among the structures were found to be higher than those between structures optimized with the dispersion contribution and in an overestimation of cell parameters and volume with respect to experimental data.

The vibrational features were assessed calculating the vibrational frequencies of the CO_3^{2-} group in the twelve structures of Figure 2. Results are reported in Table 2. For selected structures, a full vibrational analysis, *i.e.* including all CAp atoms, confirmed that they are all true minima as no imaginary frequency resulted.

According to a previous interpretation of the calculated infrared spectrum of A-type CAp, the carbonate vibrational modes were assigned as follows: in plane bending (ν_{4a} and ν_{4b}, two modes), out-of-plane bending (ν_2, one mode) and asymmetric stretching (ν_{3a} and ν_{3b}, two modes).[18] Table 2 shows the average calculated frequencies along with their standard deviation (for completeness, the IR inactive symmetrical stretching frequency ν_1 is

also reported). As expected from the low energy differences among the structures, the vibrational modes are practically independent of the carbonate orientation, as indicated by the small standard deviation values. Moreover, despite the expected systematic error in the absolute frequency values due to the adopted method, the calculated vibrational frequencies reproduce the experimental trends for both synthetic and bone A-type carbonate apatite (for further details see ref.[18]). Most importantly, the frequency difference between ν_{3a} and ν_{3b} modes resulted to be 90 cm^{-1} in very good agreement with the experimental value of 80 cm^{-1}.

Dynamic and kinetic features

Ab initio molecular dynamics (AIMD) simulations were conducted in order to assess whether the carbonate group disordering around the *c* axis has a dynamic or a static nature at room temperature, *i.e.* whether the group is almost free to rotate around the *c* axis or its orientation is restricted to a confined portion of the circumference. In a previous work Peroos et al.[9] reported, by means of classical NVT molecular dynamics simulation, a marked mobility of the CO_3^{2-} group around the *c* axis along with a less pronounced mobility in a direction perpendicular to the *c* axis.

It is worth noting that our simulations were conducted within the isobaric-isothermal (NPT) ensemble in order to take into account the essential structural relaxation of the cell consequent to the carbonate ion motion (*vide supra*). AIMD confirms the classical MD results: Figure 4 reports the carbonate ion mobility during a simulation run at 300 K for 10 ps. During the considered time span, the carbonate ion covers approximately 210° in its motion around the *c* axis, visiting at least 8 of the stable configurations found by static calculations. This suggests a very low energy barrier among the various minimum energy configurations and, consequently, a practically free rotation, confirming the dynamic nature of the carbonate group disordering. Limited carbonate mobility in and out the *ab* plane was also observed, in accordance with the classical results.

Figure 5 reports the changes of *a* and *b* parameters with respect to time (only a small time window is shown for clarity): the anti-correlation of the two cell vectors during carbonate rotation is apparent which confirms the behaviour already predicted by the static simulations (Figure 3). For some snapshots, the two lines cross, suggesting that the equivalence of the experimental *a* and *b* cell parameters results from the cell size averaging

over time which is strongly correlated to the carbonate rotation, in agreement with the static calculations. It is noteworthy that running AIMD simulations in the NVT ensemble, *i.e*. keeping the unit cell volume fixed, showed a much restricted motion of the carbonate group compared to results at NPT, implying that the subtle correlation between *a* and *b* values is a key process for the prediction of the correct unit cell symmetry.

A further insight of the CO_3^{2-} mobility can be assessed by the knowledge of the kinetic barrier hindering the rotation between two subsequent minima. To compute such a barrier, the atomic coordinates and cell parameters were interpolated between the optimized configurations 9 and 10 of Figure 2, generating a possible CO_3^{2-} rotation reaction path envisaging 10 different intermediate structures. By fitting the B3LYP-D* single point energy values for each intermediate structure we estimated an energy barrier value of 15 kJ/mol, corresponding to an Arrhenius reaction rate constant of ~10^9 s^{-1}, at room temperature. Considering that no geometry optimization has been performed along the path, the computed energy barrier value is overestimated, further confirming that the carbonate group can almost freely rotate around the *c* axis at standard conditions.

Conclusions

A-type carbonate apatite can be assigned to the $P_{\bar{3}}$ space group due to a disordering of the carbonate group around the *c* axis, resulting in twelve almost equivalent minimum energy configurations, which were optimized at B3LYP-D* and characterized by a vibrational analysis. Average cell parameters calculated according to Boltzmann's distribution are in good agreement with experimental data and confirm the assignment of the structure to the $P_{\bar{3}}$ space group. *Ab initio* molecular dynamic simulations indicated that the disordering of the carbonate group has a dynamic nature, with the carbonate rotating almost barrierless around the *c* axis and visiting the twelve characterized minimum basins. The dynamic behaviour of the carbonate moiety may have implications for the bioactivity of the CAp itself as a material formed outside a bioglass when in contact with a body fluid. As the surface of CAp is involved in the complex Hench's mechanism responsible of bioglass integration with the body, we speculate that the high CO_3^{2-} mobility may be essential to alter the kinetic of the exchangeability with other anions present in the body fluid and, ultimately, to speed up the process of bone repair and integration.

Acknowledgments

MC and PU acknowledge Progetti di Ricerca di Ateneo-Compagnia di San Paolo-2011-Linea 1A, progetto ORTO11RRT5, for funding.

Table 1 Relative energies (ΔE, in kJ/mol per cell) with respect to the most stable structure (number 9), cell parameters (Å), angles (degrees) and cell volume (Å^3) of the twelve optimized A-type CAp structures (Figure 2). Average values of cell parameters and angles computed according to the Boltzmann distribution (see text for details) and experimental values[29] are also reported.

Structure	**ΔE**	***a***	***b***	***c***	**α**	**β**	**γ**	**Vol**
1	0.62	9.597	9.678	6.860	89.50	89.33	121.84	541.1
2	2.10	9.498	9.751	6.860	89.22	90.30	121.66	540.7
3	0.04	9.367	9.591	6.860	89.36	91.15	118.59	541.1
4	1.31	9.372	9.528	6.855	90.06	90.71	117.92	540.9
5	0.41	9.678	9.368	6.860	91.17	89.52	119.52	541.1
6	2.35	9.736	9.424	6.862	90.19	89.30	120.80	540.8
7	0.60	9.597	9.677	6.860	89.50	89.33	121.84	541.1
8	2.85	9.483	9.741	6.861	89.31	90.37	121.45	540.6
9	0.00	9.368	9.591	6.860	89.37	91.16	118.58	541.1
10	2.37	9.422	9.466	6.864	90.50	90.22	117.96	540.7
11	0.35	9.678	9.367	6.860	91.17	89.52	119.52	541.1
12	2.84	9.749	9.401	6.859	90.38	89.27	120.63	540.8
Mean		**9.553**	**9.546**	**6.860**	**89.98**	**90.09**	**119.86**	**541.0**
Expt.[29]		***9.521***	***9.521***	***6.872***	***90.00***	***90.00***	***120.00***	***539.5***

Table 2 Simulated harmonic and experimental vibrational modes of the CO_3^{2-} group in A-type CAp. All frequencies are expressed in cm^{-1}. See text for band assignment.

Vibrational mode	<B3LYP-D*> ± σ	Expt. Bone	Expt. Synthetic
ν_{4a}	668 ± 2	670	-
ν_{4b}	780 ± 1	750	-
ν_2	883 ± 7	878	879
ν_1	1131 ± 2	-	-
ν_{3a}	1519 ± 1	1461	1458
ν_{3b}	1609 ± 2	-	1538

Captions to the Figures

Figure 1 Views along the *c* (left) and *a* (right) axes of the unit cell of A-type CAp (reference geometry, corresponding to structure 1 in Figure 2). Unit formula: $Ca_{10}(PO_4)_6CO_3$. Phosphate groups are represented as tetrahedra.

Figure 2 View of the twelve stable carbonate configurations along the *c* axis found during the rotational scan. Structure labels refer to Table 1. Only the apatitic channel is shown, to focus on the carbonate group.

Figure 3 Cell parameters (Å) and volume ($Å^3$) of the twelve minimum energy structures. Structure labels refer to Table 1.

Figure 4 Representation of the carbonate group mobility during the 10 ps AIMD simulation (NPT ensemble at 300 K). For clarity, only the trajectory of the oxygen atom perpendicular to the *c* axis is reported. The channel of calcium ions surrounding the group is represented schematically. Larger circles represent Ca ions in the upper plane.

Figure 5 Fluctuation of the cell parameters *a* (full black line) and *b* (dashed red line) during a 2.5 ps window of the NPT AIMD simulation.

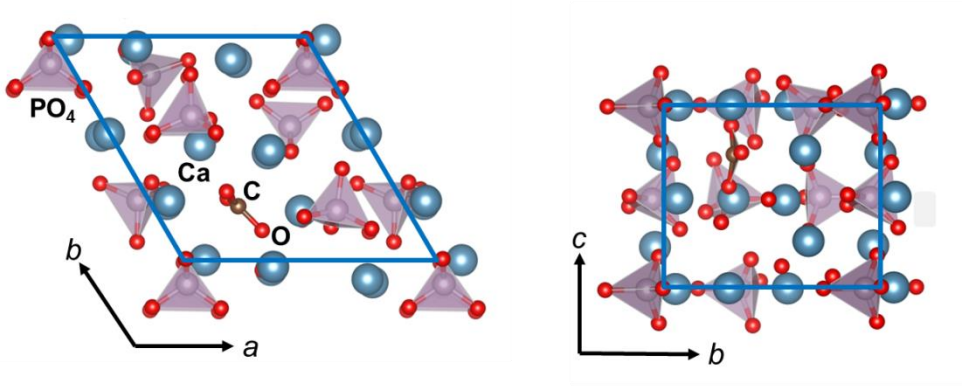

Figure 1

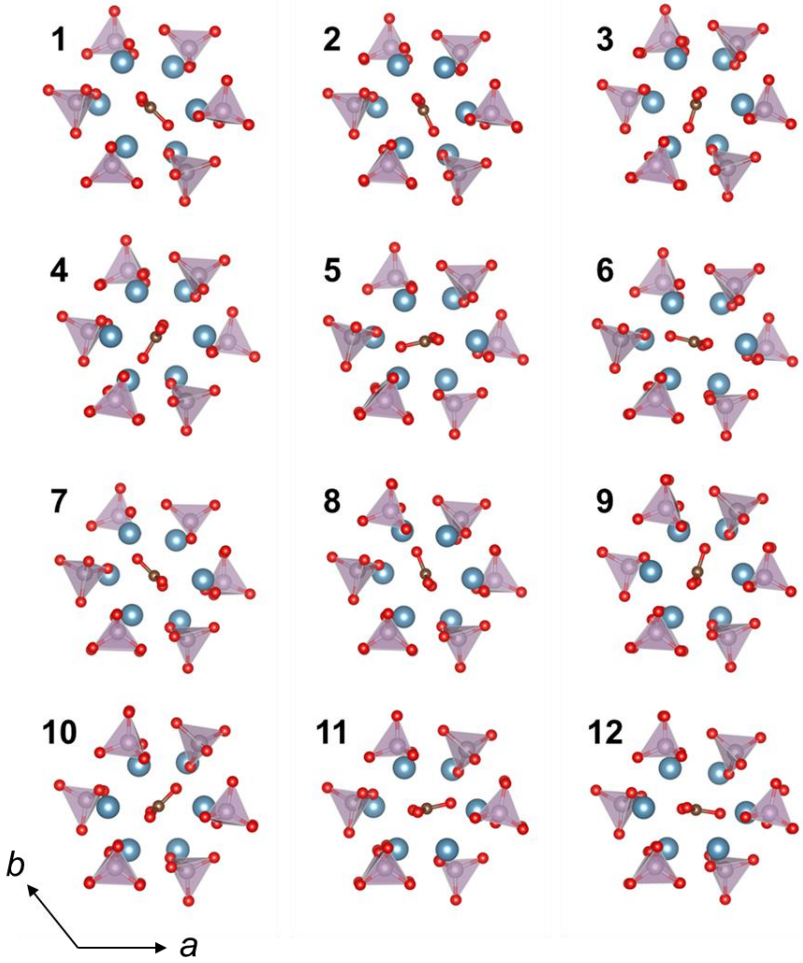

Figure 2

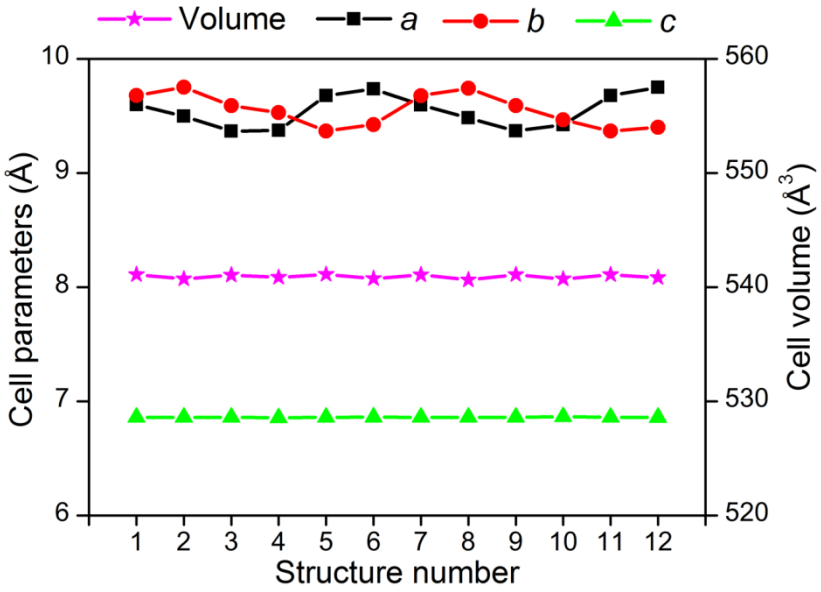

Figure 3

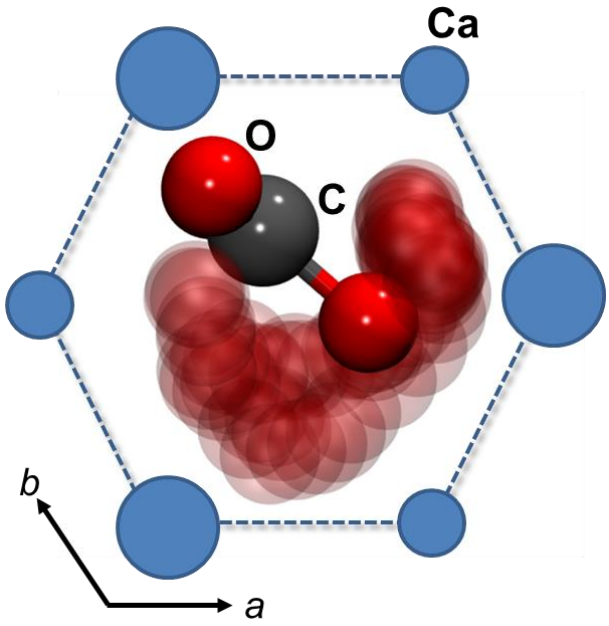

Figure 4

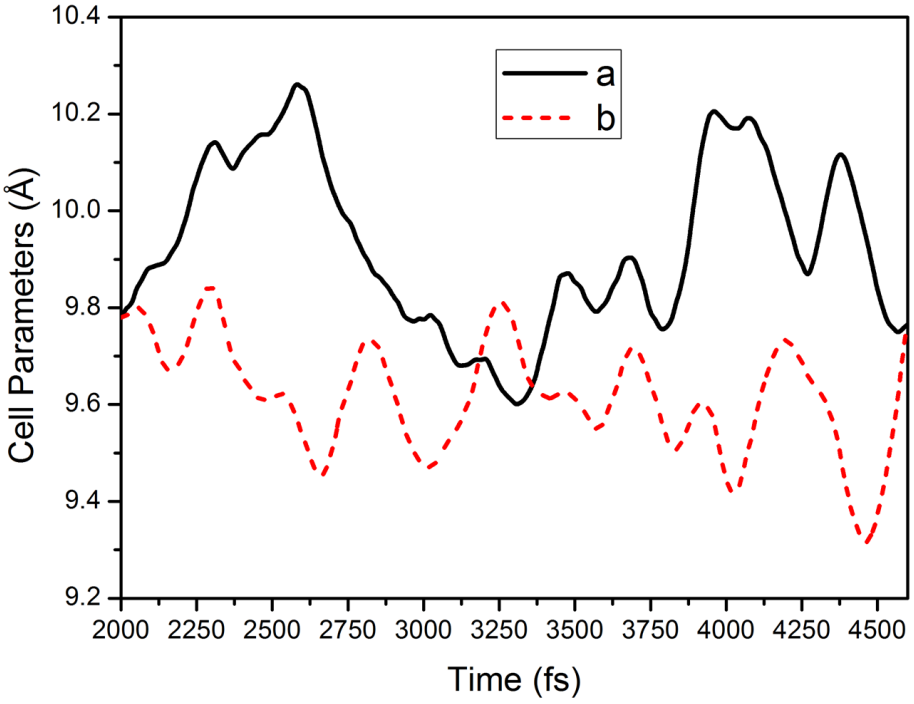
10.4
10.2
10.0
9.8
9.6
9.4
9.2
Cell Parameters (Å)
a
b
2000
2250
2500
2750
3000
3250
3500
3750
4000
4250
4500
Time (fs)

Figure 5

References

1. Dorozhkin, S. V.; Epple, M. Biological and Medical Significance of Calcium Phosphates. *Angew. Chem. Int. Ed.* **2002**, *41*, 3130-3146.

2. Wopenka, B.; Pasteris, J. D. A Mineralogical Perspective on the Apatite in Bone. *Mater. Sci. Eng. C* **2005**, *25*, 131-143.

3. Suetsugu, Y.; Shimoya, I.; Tanaka, J. Configuration of Carbonate Ions in Apatite Structure Determined by Polarized Infrared Spectroscopy. *J. Am. Ceram. Soc.* **1998**, *81*, 746-748.

4. Fleet, M. E.; Liu, X. Carbonate Apatite Type A Synthesized at High Pressure: New Space Group (P-3) and Orientation of Channel Carbonate Ion. *J. Solid State Chem.* **2003**, *174*, 412-417.

5. Fleet, M. E.; Liu, X. Orientation of Channel Carbonate Ions in Apatite: Effect of Pressure and Composition. *Am. Mineral.* **2011**, *96*, 1148-1157.

6. Ulian, G.; Valdré, G.; Corno, M.; Ugliengo, P. Periodic Ab Initio Bulk Investigation of Hydroxylapatite and Type A Carbonated Apatite with Both Pseudopotential and All-Electron Basis Sets for Calcium Atoms. *Am. Mineral.* **2013**, *98*, 410-416.

7. Astala, R.; Stott, M. J. First Principles Investigation of Mineral Component of Bone: CO_3 Substitutions in Hydroxyapatite. *Chem. Mater.* **2005**, *17*, 4125-4133.

8. Rabone, J. A. L.; de Leeuw, N. H. Potential Routes to Carbon Inclusion in Apatite Materials: A DFT Study. *Phys. Chem. Miner.* **2007**, *34*, 495-506.

9. Peroos, S.; Du, Z.; de Leeuw, N. H. A Computer Modelling Study of the Uptake, Structure and Distribution of Carbonate Defects in Hydroxy-Apatite. *Biomater.* **2006**, *27*, 2150-2161.

10. Perdew, J. P.; Burke, K.; Enzerhof, M. Generalized Gradient Approximation for the Exchange-Correlation Hole of a Many-Electron System. *Phys. Rev. Lett.* **1996**, *77*, 3865-3868.

11. Becke, A. D. Density-Functional Thermochemistry. III. The Role of Exact Exchange. *J. Chem. Phys.* **1993**, *98*, 5648-5652.

12. Lee, C.; Yang, W.; Parr, R. G. Development of the Colle-Salvetti Correlation-Energy Formula into a Functional of the Electron Density. *Phys. Rev. B* **1988**, *37*, 785-789.

13. Dovesi, R.; Saunders, V. R.; Roetti, C.; Orlando, R.; Zicovich-Wilson, C. M.; Pascale, F.; Civalleri, B.; Doll, K.; Harrison, N. M.; Bush, I. J.; D'Arco, P.; Llunell, M. *Crystal09, User's Manual*, 2009.

14. Dovesi, R.; Civalleri, B.; Orlando, R.; Roetti, C.; Saunders, V. R. Ab Initio Quantum Simulation in Solid State Chemistry. *Rev. Comp. Chem.* **2005**, *21*, 1-125.

15. Dovesi, R.; Orlando, R.; Civalleri, B.; Roetti, C.; Saunders, V. R.; Zicovich-Wilson, C. M. Crystal: A Computational Tool for the *Ab Initio* Study of the Electronic Properties of Crystals. *Z. Kristallogr.* **2005**, *220*, 571-573.

16. Bush, I. J.; Tomic, S.; Searle, B. G.; Mallia, G.; Bailey, C. L.; Montanari, B.; Bernasconi, L.; Carr, J. M.; Harrison, N. M. Parallel Implementation of the Ab Initio Crystal Program: Electronic Structure Calculations for Periodic Systems. *Proc. R. Soc. A-Math. Phys. Eng. Sci.* **2011**, *467*, 2112-2126.

17. Orlando, R.; Delle Piane, M.; Bush, I. J.; Ugliengo, P.; Ferrabone, M.; Dovesi, R. A New Massively Parallel Version of Crystal for Large Systems on High Performance Computing Architectures. *J. Comput. Chem.* **2012**, *33*, 2276-2284.

18. Ulian, G.; Valdre, G.; Corno, M.; Ugliengo, P. The Vibrational Features of Hydroxylapatite and Type A Carbonated Apatite: A First Principle Contribution. *Am. Mineral.* **2013**, *98*, 752-759.

19. Monkhorst, H. J.; Pack, J. D. Special Points for Brillouin-Zone Integration. *Phys. Rev. B.* **1976**, *8*, 5188-5192.

20. Dall'Olio, S.; Dovesi, R.; Resta, R. Spontaneous Polarization as a Berry Phase of the Hartree-Fock Wave Function: The Case of $KnBO_3$. *Phys Rev B* **1997**, *56*, 10105-10114.

21. Grimme, S. Semiempirical GGA-Type Density Functional Constructed with a Long-Range Dispersion Correction. *J. Comput. Chem.* **2006**, *27*, 1787-1799.

22. Civalleri, B.; Zicovich-Wilson, C. M.; Valenzano, L.; Ugliengo, P. B3LYP Augmented with an Empirical Dispersion Term (B3LYP-D*) as Applied to Molecular Crystals. *CrystEngComm* **2008**, *10*, 405-410.

23. Kohlmeyer, A.; Mundy, C. J.; Mohamed, F.; Schiffmann, F.; Tabacchi, G.; Forbert, H.; Kuo, W.; Hutter, J.; Krack, M.; Iannuzzi, M.; McGrath, M.; Guidon, M.; Kuehne, T. D.; Laino, T.; VandeVondele, J.; Weber, V. CP2K program **2004**.

24. VandeVondele, J.; Krack, M.; Mohamed, F.; Parrinello, M.; Chassaing, T.; Hutter, J. Quickstep: Fast and Accurate Density Functional Calculations Using a Mixed Gaussian and Plane Waves Approach. *Comput. Phys. Commun.* **2005**, *167*, 103-128.

25. Lippert, G.; Hutter, J.; Parrinello, M. A Hybrid Gaussian and Plane Wave Density Functional Scheme. *Mol. Phys.* **1997**, *92*, 477-488.

26. Hartwigsen, C.; Goedecker, S.; Hutter, J. Relativistic Separable Dual-Space Gaussian Pseudopotentials from H to Rn. *Phys. Rev. B* **1998**, *58*, 3641-3662.

27. Bussi, G.; Donadio, D.; Parrinello, M. Canonical Sampling through Velocity Rescaling. *J. Chem. Phys.* **2007**, *126*, 014101.

28. Corno, M.; Orlando, R.; Civalleri, B.; Ugliengo, P. Periodic B3LYP Study of Hydroxyapatite (001) Surface Modelled by Thin Layer Slabs. *Eur. J. Min.* **2007**, *19*, 757-767.

29. Fleet, M. E.; Liu, X. Local Structure of Channel Ions in Carbonate Apatite. *Biomater.* **2005**, *26*, 7548-7554.

TOC Table of contents Graphics